RESEARCH ARTICLE

Discovery and Characterization of Novel Naphthalimide Analogs as Potent Multitargeted Directed Ligands against Alzheimer's Disease

Jie Gao[1] | James Chapman[2]

[1]Department of Clinical and Diagnostic Science, University of Alabama at Birmingham, Birmingham, Alabama, USA

[2]Department of Discovery and Biomedical Sciences, University of South Carolina, Columbia, South Carolina, USA

Correspondence
Jie Gao, Department of Clinical and Diagnostic Science, University of Alabama at Birmingham, 1716 9th Ave. S, Birmingham, AL 35294.
Email: gaoj@uab.edu

Abstract

Current therapeutic drugs for Alzheimer's disease (AD) can only offer limited symptomatic benefits and do not halt disease progression. Multitargeted directed ligands (MTDLs) have been considered to be a feasible way to treat AD due to the multiple neuropathological processes in AD. Previous studies proposed that compounds containing two aromatic groups connected by a carbon chain should act as effective amyloid β (Aβ) aggregation inhibitors although the optimal length of the carbon chain has not been explored. In the current study, a series of naphthalimide analogs were designed and synthesized based on the proposed structure and multiple bioactivities beneficial to the AD treatment were reported. *In vitro* studies showed that compound 8, which has two aromatic groups connected by a two-carbon chain, exhibited significant inhibition of Aβ aggregation through the prevention of elongation and association of Aβ fibril growth. Furthermore, this compound also displayed antioxidative activities and neuroprotection from Aβ monomer induced toxicity in primary cortical neurons. The results of the present study highlight a novel naphthalimide-based compound 8 as a promising MTDL against AD. Its structural elements can be further explored for enhanced therapeutic capabilities.

KEYWORDS

Alzheimer's disease, amyloid aggregation, amyloid-β protein, antioxidation, multitargeted directed ligands, naphthalimide, neuroprotection, oxidative stress

1 | INTRODUCTION

Alzheimer's disease (AD) is a widely known to be a result of many pathological factors such as amyloid plaques and oxidative stress (Hardy & Allsop, 1991; Su et al., 2008). Aβ aggregation is one of the most widely studied pathological factors involved in AD. Aβ peptides are ~4.3 kDa proteins produced by normal brain metabolism. Two major Aβ variants, $A\beta_{40}$ and $A\beta_{42}$, have been identified as the principal pathological species in amyloid plaques deposited in the AD brain, and $A\beta_{40}$ is the most plentiful isoform in amyloid plaques (Guntert, Dobeli, & Bohrmann, 2006; Walsh & Selkoe, 2007). The aggregation process of Aβ monomers has been described as three steps: nucleus formation, soluble aggregates, and fibril formation (Goedert & Spillantini, 2006). The soluble Aβ aggregates can grow into fibrils through elongation or association. The elongation growth increases aggregate size through the addition of Aβ monomers to the ends of the aggregates and results in fibrils with a mass-per-unit length similar to the staring material. The association growth increases Aβ

ABBREVIATIONS: AD, Alzheimer's disease; Aβ, amyloid β; BSA, bovine serum albumin; DLS, dynamic light scattering; DMSO, dimethyl sulfoxide; MTDL, multitargeted directed ligands; mtDNA, mitochondrial DNA; ORAC, oxygen radical absorbance capacity; PBS, phosphate buffered saline; Phe, phenylalanine; R_H, hydrodynamic radius; ROS, reactive oxygen species; SEC, size exclusion chromatography; TEM, transmission electron microscopy; ThT, thioflavin T.

aggregates in size direct lateral aggregate–aggregate interactions and leads to increase in aggregate size with a larger mass-per-unit length ratio than the starting aggregate (Nichols et al., 2002).

Oxidative stress has also been identified as an early event in the pathogenesis of AD (Padurariu et al., 2010). The important sources of oxidative stress, reactive oxygen species (ROS) and reactive nitrogen oxide species (RNOS), can particularly react with lipids, proteins, nucleic acid, and other molecules in brain and cause a significant extent of oxidative damage associated with the abnormal deposition of both Aβ aggregates and neurofibrillary tangles in AD (Mattson, 2004). Therefore, antioxidants have been suggested to be a viable option to not only prevent Aβ aggregation, but also address some other pathological factors such as mitochondrial dysfunction, neuronal inflammation, and so on. Some commonly used antioxidants have been studied for their useful indications in the therapeutic treatment of AD (Feng & Wang, 2012).

These concurrent mechanisms contribute to the progression of AD and are likely to be highly interrelated (Carreiras, Mendes, Perry, Francisco, & Marco-Contelles, 2013). Current AD therapies are single targeted drugs such as acetylcholinesterase inhibitors (donepezil, rivastigmine, and galantamine) and the NMDA receptor antagonist (memantine). However, the interactions among the different pathological factors preclude the effectiveness of these single targeted drugs, which only offer symptomatic benefits for mild to moderate AD but without halting or delaying disease progression (Yiannopoulou & Papageorgiou, 2013). Therefore, multitarget-directed ligands (MTDL), which can address different pathological targets simultaneously without the risk of drug–drug interactions, have been proposed to be one of the ideal treatments for AD (Cavalli et al., 2008) and have also been exploited at both academic and industrial levels. (Goyal, Kaur, & Goyal, 2018; Kaur et al., 2019; Kaur, Shuaib, Goyal, & Goyal, 2020; Patil, Thakur, Sharma, & Flora, 2019; Yang et al., 2020).

During the development of disease modifying drugs for AD, the prevention of Aβ aggregation at different steps has become one of

most useful strategies. Various compounds such as curcumin, rifampicin, benzofuran, and bis-styrylbenzene analogs have been explored as Aβ aggregation inhibitors (Byun et al., 2008; Lee et al., 2008; Narlawar, Baumann, Schubenel, & Schmidt, 2007; Ono, Hasegawa, Naiki, & Yamada, 2004). In particular, the dipeptide (Phe19-Phen20) in the Aβ monomer was reported to play a critical role in the formation of soluble aggregates (Tjernberg et al., 1996), therefore, the analogic structure of this dipeptide, two aromatic end groups connected by a linker, has been proposed as an ideal scaffold of Aβ aggregation inhibitors. These analogs are hypothesized to inhibit the Aβ aggregation through the interactions to the phenylalanine residues 19 and 20, which disrupt the π–π stacking between Aβ monomers (Reinke & Gestwicki, 2007). According to this proposed structure, numerous potential inhibitors have been studied and demonstrated potent inhibition of Aβ aggregation (Kroth et al., 2012; McKoy, Chen, Schupbach, & Hecht, 2012; Nie, Du, & Geng, 2011).
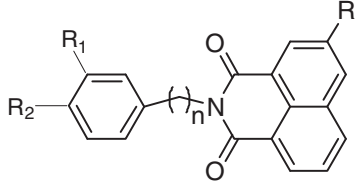
Naphthalimides have been reported to serve as core scaffold for many antitumor, anti-inflammatory, antidepressant, antiprotozoal, and antiviral agents, and some of which were found without obvious systemic toxicities at the therapeutic dose (Kamal, Bolla, Srikanth, & Srivastava, 2013; Xie et al., 2012). Therefore, in the current study, we rationally designed and developed a series of naphthalimide compounds, which combine Aβ aggregation inhibition, neutralization of oxidative stress and neuroprotection, as MTDLs against AD.

2 | RESULTS AND DISCUSSION

2.1 | Inhibition of Aβ monomer aggregation

The inhibitory activities of the naphthalimide analogs to Aβ aggregation are summarized in Table 1 regarding both lag time extension and plateau reduction. Synthetic $A\beta_{40}$ was used in this study because the structure of $A\beta_{40}$ fibrils formed using synthetic monomers is similar to

TABLE 1 The structure of naphthalimide analogs and their inhibition capability on Aβ monomer aggregation

Compound	n	R	R_1	R_2	Plateau reduction (% inhibition)	Lag extension (fold increase)	ORAC activity
1	1	H	H	H	17.4 ± 2.9	NE	NT
2	1	NO_2	H	H	24.4 ± 5.6	NE	NT
3	2	H	H	H	39.7 ± 8.6	2.4 ± 0.7	NT
4	3	H	H	H	22.9 ± 9.7	NE	NT
5	3	NO_2	H	H	37.4 ± 2.9	NE	NT
6	4	H	H	H	34.0 ± 5.2	NE	NT
7	2	H	H	OH	35.2 ± 5.1	NE	0.52 ± 0.22
8	2	H	OH	OH	85.2 ± 2.9	4.9 ± 1.6	1.22 ± 0.33

Abbreviations: NE, the results of compounds at 100 μM are not significantly different from the ones of control samples; NT, not tested.
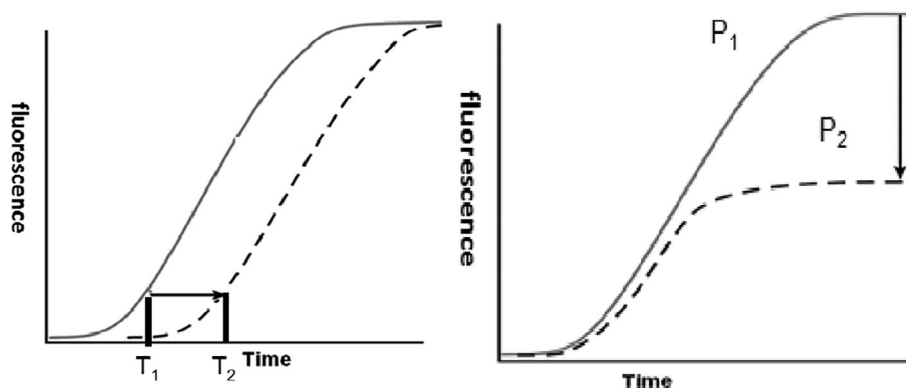
FIGURE 1 Assessment of inhibition of Aβ monomer aggregation by naphthalimide analogs. Monomer aggregation assays were conducted in the absence (solid line, control) and presence (dotted line, experimental) of the naphthalimide analogs. Aggregate formation was monitored using ThT fluorescence to evaluate the ability of each compound to alter the lag time and plateau. Extension of lag time was proved as an increase in the experimental lag time, T_2, relative to the lag time for the control, T_1, and evaluated as a fold increase to the control, T_2/T_1 (left panel). Reduction of control plateau was evidenced as an decrease in the experimental plateau, P2, relative to the plateau for the control, P1, and evaluated as the percentage decrease to the control, $[(P1 - P2)/P1] \times 100\%$ (right panel)
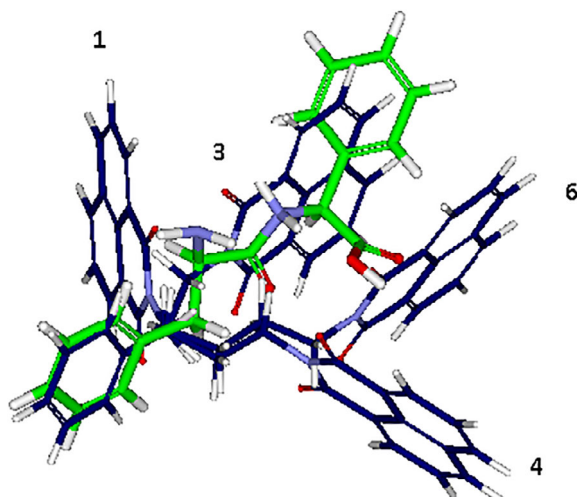

FIGURE 2 The alignment of compound 1, 3, 4, and 6 (blue) and the Phe-Phe peptide (green) in the most energetically favorable computed conformations

TABLE 2 The lengths and angles of the two aromatic groups within compound 1, 3, 4, and 6

Compound	Length between two aromatic groups[a]	Angles between two aromatic groups[a]
Phe-Phe	8.525 Å	173.81°
1	6.470 Å	112.66°
3	8.752 Å	179.70°
4	8.826 Å	167.83°
6	8.976 Å	170.86°

[a]The length of the linkers and the angles of the two aromatic groups are measured by Discovery Studio 2.5 (Accelrys, San Diego, CA).

fibrils isolated from amyloid plaques (Goedert & Spillantini, 2006). The production of Aβ aggregates had been measured through the equilibrium plateau (indicating the amount of aggregated forms) and the lag time (indicating the delay of Aβ aggregate production) (Figure 1), which are normally monitored by thioflavin T (ThT), a fluorescent compound specifically binding to the β-sheet structures in the Aβ aggregates. The lag time extension, which occurs in the early stages of Aβ aggregation, was determined as the fold increase of the time at which ThT fluorescence is first increased in the presence and absence of inhibitor, T1 and T2, respectively (Figure 1, left panel). The plateau reduction, which occurs in the late points of Aβ aggregation, was defined as the percentage decrease of the plateau ThT fluorescence in the presence of inhibitor, P2, compared to the plateau observed in the absence of inhibitor, P1 (Figure 1, right panel). It should be noted that compound 3, containing a two-carbon chain between the two

aromatic rings, significantly extended the lag time by 2.4 ± 0.7 folds over the control sample, which indicated that the two-carbon chain might be a proper length for 1,8-naphthalimide analogs as Aβ inhibitors. The lag time extension of compound 3 might be due to its conformational compatibility to Phe19-Phe20 in Aβ peptide, which interfered the initial binding of Aβ monomers at the early stage. Therefore, compound 1, 3, 4, and 6 in their most energetically favorable computed conformations were aligned to one of the phenyl rings in Phe19-Phe20 with the help of the Discovery Studio 2.5, a software that simulates small molecules and macromolecules systems. The aligned result is shown in Figure 2 and the lengths and angles of the two aromatic rings within the compounds are listed in Table 2. As shown in the Table 2, the two aromatic rings in compound 3 possess a length of 8.752 Å and an angle of 179.70°, both of which are similar to the ones of Phe19-Phe20 (8.525 Å and 173.81°, respectively). This conformation of compound 3 leads the 1,8-naphthalimide ring to a similar direction to the Phe19-Phe20 peptide (green, Figure 2). These molecular modeling results supported the experimental data that compound 3 can hinder the Phe19-Phe20 binding between Aβ monomers and effectively delay the Aβ aggregate formation.

In order to increase the plateau inhibition of Aβ aggregation and the antioxidant activity of compound 3, hydroxyl groups were added

to its structure and offered compound 7 and 8. The compound 8 with two hydroxyl groups presents significant Aβ aggregation inhibition with a plateau reduction of 85.2 ± 2.9% and a lag time extension of 4.9 ± 1.6 folds over the control sample. The results of compound 7 and 8 indicated that 3-hydroxyl substitution may be more critical for potent inhibitory activities than 4-hydroxyl substitution on phenyl rings. It might also be conceivable that at least two hydroxyl groups are required to exhibit potent Aβ aggregation inhibition.

Based on these compounds evaluated as Aβ aggregation inhibitors, the preliminary structure activity relationship could be summarized as: (a) the addition of a nitro group on the naphthalimide phenyl ring does not potentiate the Aβ aggregation inhibition; (b) a two-carbon chain might possess the optimal length in these 1,8-naphthalimide molecules for lag time extension instead of plateau reduction; and (c) The presence of two or more phenol groups in the naphthalimide structure can significantly potentiate the molecular activity to inhibit Aβ aggregation.

2.2 | The mechanistic-specific inhibition of compound 8

In order to explore the inhibitory mechanisms of compound 8, the soluble Aβ aggregates increase in size via association or elongation was monitored as the change in hydrodynamic radius (R_H). As shown in Figure 3a, whereas Aβ monomer or soluble aggregates incubated alone exhibited negligible changes in R_H, a steady increase in R_H was observed when soluble Aβ aggregates (2 μM) were incubated in the presence of Aβ monomer. However, when the same soluble Aβ aggregates were incubated with compound 8 (80 μM) before the addition of Aβ monomer, the observed elongation rate, or rate of increase in R_H, was reduced by 75.3 ± 9.5%, which meant that compound 8 significantly inhibited the elongation of soluble Aβ aggregates. Similarly, Figure 3b showed a steady increase in R_H when the aggregates were incubated in the presence of NaCl. When 2 μM soluble Aβ aggregates were incubated with compound 8 (10 μM) before the addition of
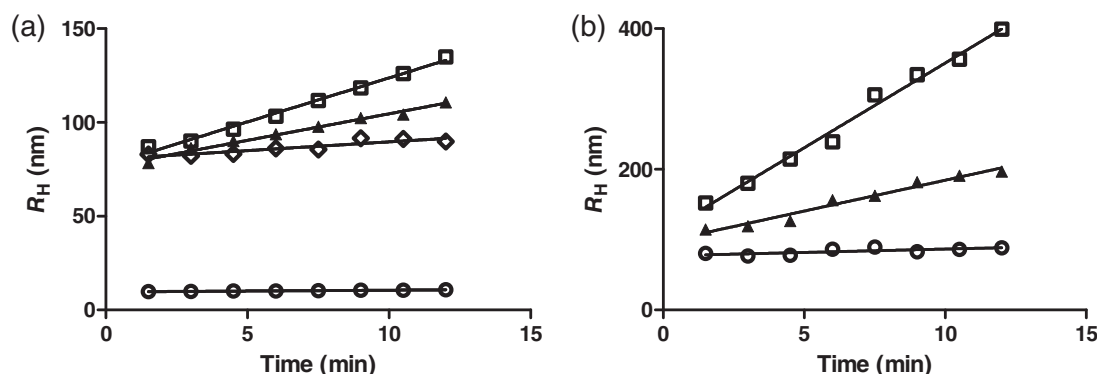
FIGURE 3 Effect of compound 8 on soluble Aβ soluble aggregate growth. (a) soluble Aβ aggregates (2 μM) with positive control (0 μM, □), or compound 8 (80 μM,▲), and Aβ monomer (30 μM) was added to induce aggregate growth. As negative controls, the soluble Aβ aggregates (◇) or Aβ monomer (○) were incubated alone. Increases in aggregate size were monitored continuously as changes in R_H. (b) soluble Aβ aggregates (2 μM) with positive control (0 μM, □), or compound 8 (10 μM, ▲), and 150 mM NaCl was added to induce aggregate association. As a negative control, the soluble Aβ aggregates (○) were incubated alone and in the absence of NaCl. Increases in aggregate size were monitored continuously as changes in R_H. Linear regression (solid lines) was performed to determine association growth rates (r^2). Results are representative of three independent experiments
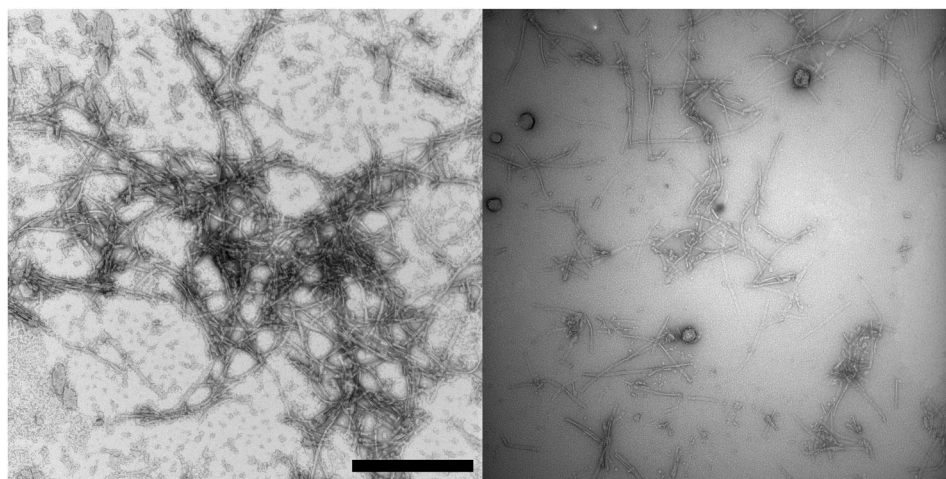
FIGURE 4 Morphology of Aβ$_{1-40}$ aggregates. SEC-isolated Aβ monomers in 40 mM Tris–HCl, pH 8.0, were aggregated alone (control, left panel) or with compound 8 (100 μM, right panel). After control reached plateau, the reactions were terminated and samples were gridded and visualized by TEM as described under experimental section. Results are representative of two independent experiments. Images are shown relative to a scale bar of 0.5 μm

NaCl, the observed association rate, or rate of increase in R_H, was reduced by 75.2 ± 11.4%, which indicates a potent inhibition on the association of Aβ aggregate. The presence of 2% DMSO has a negligible effect on the growth of the soluble Aβ aggregates by association (data not shown).

In order to visualize the formation and morphological changes of Aβ fibrils, the transmission electron microscopy (TEM) was employed to acquire direct images of Aβ aggregates. Figure 4 depicted the Aβ fibril images when Aβ monomers were incubated with NaCl alone (left) or in the presence of NaCl and compound 8 (right). Both pictures showed fibrillar aggregates but with some notable differences. For example, there are less fibrils were formed in the presence of compound 8 (right). The fibrils are shorter and thinner in this picture than the ones in the left picture. This observation backed up the fact that compound 8 prevents the production of Aβ fibrils from monomers through the inhibition of both elongation and association.

2.3 | Antioxidative activity of compound 7 and compound 8

The antioxidative activity of compound 7 and 8 was evaluated by the oxygen radical absorbance capacity (ORAC) assay and the inducible nitric oxygen synthase (iNOS) induction assay. In the ORAC assay, the antioxidative activity was evaluated based on the ORAC values. The ORAC value of the control agent Trolox is designed as 1 and the values of the testing compound will compare to Trolox. As shown in Table 1, compound 8 with the ORAC value of 1.22 ± 0.33 demonstrated a more potent antioxidative activity than Trolox. Consistent with the ORAC data, compound 8 can also significantly suppress the production of iNOS induced by IFN-γ at 8 hr (Figure 5). These data indicated that compound 8 has a potent antioxidative activity against oxidative damages in addition to the Aβ aggregation inhibition.
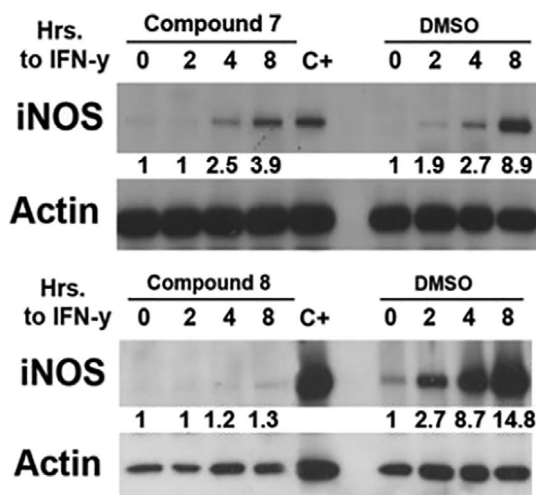

FIGURE 5 Effects of compounds 7 (100 μM) and compound 8 (100 μM) on the induced expression of iNOS. C+ (positive control) was an archived ANA-1 cell lysate known to have iNOS induction. Numbers under each band represent the densitometric quantification of iNOS bands, and adjusted for Actin levels
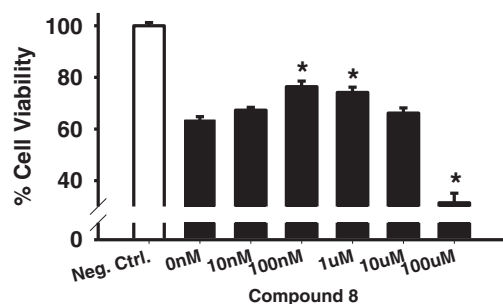
2.4 | Neuroprotective activity of compound 8

Compound 8 was further tested on primary cortical neuronal cultures to assess the potential neuroprotective effects against the compromised neuronal viability induced by the Aβ monomers. As shown in Figure 6, 24 hr incubation with the Aβ monomers (200 nM) decreased cell survival by about 40% in each series of experiments. Compound 8 significantly increased the cell viability around 80% of control values at the concentrations of 100 nM and 1 μM although extremely high concentration (10 μM) of the compound demonstrates toxic activity. It has been reported that phenolic compounds can protect neurons from amyloid challenges through multiple mechanisms such as the inhibition of NADPH oxidase and subsequent reactive oxygen species generation, the reduction of inflammation, and so on (Kovacsova, Andrej, Jana, Stanislava, & Olga, 2010). Effectiveness of compound 8 might also attribute to these mechanisms. Its structural features may aid the rational drug design approaches in future.

2.5 | Drug likeness of compound 8

Several physiochemical properties of compound 8 related drug likeness were calculated by QikProp, version 3.5, Schrödinger, LLC (2015). The virtual screening results indicate that compound 8

FIGURE 6 Neuroprotective effects of compound 8 against Aβ monomer (200 μM) as determined in a cell viability assay in rat cortical neuron primary culture

TABLE 3 Compliance of Compound 8 with computational parameters of drug likeness

Compound	Molecular weight (kD)	CLogP	acceptHB	donorHB	Rule of 5 violation
8	333	2.8	4.5	2	0

Abbreviations: CLogP, calculated logP; acceptHB, estimated number of hydrogen bonds acceptor; donorHB, estimated number of hydrogen bonds donor.

TABLE 4 The standard computational parameters of pharmacokinetics for Compound 8

Compound	LogS (mol/ml)	LogKhsa	CNS	Caco	LogBB
8	−4.3	0.24	−2	259	−1.3
Standard range[a]	−6.5–0.5	−1.5–1.5	−2 (inactive) +2 active)	<25 poor >500 great	−3.0–1.2

Abbreviations: Caco, predicted apparent Caco-2 cell permeability in nm/sec; CNS, Predicted central nervous system activity; LogBB, predicted brain/blood partition coefficient; LogS, prediction of aqueous solubility; LogKhsa, prediction of binding to human serum albumin.
[a]For 95% of known drugs based on Schrödinger—Qikprop v3.5 (2015) software results.

followed the modified Lipinski's "Rule of Five" for CNS drug likeness properties (Table 3). In addition, its pharmacokinetics parameters such as aqueous solubility (LogS), serum protein binding (LogKhsa), and gut-blood barrier (Caco-2 cell permeability) were within the standard ranges of 95% known drugs (Table 4), although its distribution to the central nervous system was predicted to be poor based on the logBB and the predicted central nervous system activity (CNS). It has been documented that the estimated number of hydrogen bond donors should be less than 1 for CNS drugs (Ghose, Herbertz, Hudkins, Dorsey, & Mallamo, 2012). This poor distribution to CNS might be due to the phenolic groups, which provided two active hydrogen bond donors and significantly decreased its penetration to BBB. A number of studies reported various approaches to make prodrugs in order to improve phenolic drug deliveries (Placzek et al., 2016; Thomas, Majumdar, & Sloan, 2009; Valiveti et al., 2005). Therefore, as a promising leading compound, the CNS activity of compound 8 could be improved through prodrugs.

3 | CONCLUSIONS

AD is set to become even more prevalent as the average age of the population continues to increase. Valid AD treatment discovery is a crucial issue for both pharmaceutical industries and academia. In this study, a series of 1,8-naphthalimide analogs were designed and synthesized as a new type of structural scaffold for multiple potent biological activities including Aβ aggregation inhibition, antioxidant effect and neuroprotectivity, which might be favorable for further structural modification and drug development against AD. Of these compounds evaluated herein, compound 8 was found to effectively inhibit Aβ aggregation and oxidative damages; and also associated with modest neuroprotective effects from toxicity induced by Aβ monomers in the primary neuronal culture model. Together, compound 8 provided structural information for an optimal scaffold of MTDL in the drug development of AD.

4 | EXPERIMENTAL

4.1 | Materials and general methods

Unlabeled and *N*-terminally biotinylated Aβ were purchased from AnaSpec (Fremont, CA) and were stored in lyophilized formed at −20°C.

Thioflavin T (ThT) was obtained from Sigma (St. Louis, MO). Bovine serum albumin (BSA) and dimethyl sulfoxide (DMSO) were purchased from EMD Biosciences (San Diego, CA). Tris–HCl buffer was made of tris base, purchased from Promega (Madison, WI) and tris hydrochloride, purchased from EMD (Philadelphia, PA) with a pH value of 8.0.

4.2 | Chemical synthesis

Melting points were determined on an Electrothermal® melting point apparatus (capillary method) and are uncorrected. 1H-NMR spectra were obtained on Mercury VX-300 spectrometer (Varian), using deuterochloroform (CDCl₃) as the solvent. Most chemicals were purchased from Acros Organics and TCI America chemicals. Mass spectrometry was performed utilizing a VG Analytical 70S magnetic sector mass spectrometer (waters, Milford Mass). Chromatography was performed using Geduran® silica gel (40-63 μm).

1,8-naphthalimide analogs (compound 1–8).

To a suspension of 1,8-naphthalic anhydride (3.0 g, 15 mmol) in toluene (100 mL), the corresponding reactants (15 mmol) were added dropwise. The reaction mixture was refluxed with a condenser and a Dean-Starke trap for 5 hr and then evaporated to yellow solid, which was recrystallized with toluene (60 mL) to yield products.

2-Benzyl-1H-benzo[de]isoquinoline-1,3(2H)-dione(1) mp:194–196°C. 1H NMR(300 MHz, CDCl₃) δ 5.32 (s, 2H, C*H*₂N), 7.16–7.26(m, 4H, ArH), 7.48(d, 1H, J = 7.2, ArH), 7.68(t, J = 8.4, 2H, ArH), 8.13(d, J = 8.4, 2H, ArH), 8.54(d, J = 7.2, 2H, ArH). HRMS: Obs. M + H, 287.0942. Calc. M + H, 287.0946.

2-Benzyl-5-nitro-1H-benzo[de]isoquinoline-1,3(2H)-dione(2) mp:194–196°C.1H NMR(300 MHz, CDCl₃) δ 5.40 (s, 2H, C*H*₂N), 7.28–7.34(m, 3H, ArH), 7.55(d, J = 7.2, 2H, ArH), 7.94(t, J = 7.8, 1H, ArH), 8.42(d, J = 8.4, 1H, ArH), 8.79(d, J = 7.2, 1H, ArH), 9.13(s, 1H, ArH), 9.34(s, 1H, ArH). HRMS: Obs. M + H, 332.0797. Calc. M + H, 332.0797.

2-Phenethyl-1H-benzo[de]isoquinoline-1,3(2H)-dione(3) mp:127–128°C. 1H NMR(300 MHz, CDCl₃) δ 2.96 (m, 2H, C*H*₂CH₂N), 4.34(m, 2H, CH₂C*H*₂N), 7.14–7.33(m, 5H, ArH), 7.70(t, J = 7.5, 2H, ArH), 8.16(d, J = 8.1, 2H, ArH), 8.54(d, J = 7.2, 2H, ArH). HRMS: Obs. M + H, 301.1100. Calc. M + H, 301.1103.

2-(3-Phenylpropyl)-1H-benzo[de]isoquinoline-1,3(2H)-dione(4) mp:88–89°C.1HNMR (300 MHz, CDCl₃) δ 1.99 (m, 2H, CH₂C*H*₂CH₂N), 2.71(t, J = 7.5, 2H, C*H*₂CH₂CH₂N), 4.19(t, J = 7.5, 2H, CH₂CH₂C*H*₂N), 7.05–8.00(m, 1H, ArH), 7.17–7.19(m, 4H, ArH), 7.69

(t, J = 7.5, 2H, ArH), 8.14(d, J = 8.1, 2H, ArH), 8.53(d, J = 7.5, 2H, ArH). HRMS: Obs. M + H, 315.1255. Calc. M + H, 315.1259.

5-Nitro-2-(3-phenylpropyl)-1H-benzo[de]isoquinoline-1,3(2H)-dione(5) mp:128–129°C. 1H NMR(300 MHz, CDCl$_3$) δ 2.04 (m, 2H, CH$_2$CH$_2$CH$_2$N), 2.72(t, J = 8.1, 2H, CH$_2$CH$_2$CH$_2$N), 4.20(t, J = 7.5, 2H, CH$_2$CH$_2$CH$_2$N), 7.04(m, 1H, ArH), 7.15–7.19(m, 4H, ArH), 7.87(t, J = 7.8, 1H, ArH), 8.35(d, J = 8.1, 1H, ArH), 8.70(d, J = 7.1, 1H, ArH), 9.06(d, J = 2.1, 1H, ArH), 9.24(d, J = 2.1, 1H, ArH). HRMS: Obs. M + H, 360.1105. Calc. M + H, 360.1110.

2-(4-Phenylbutyl)-1H-benzo[de]isoquinoline-1,3(2H)-dione(6) mp:108–109°C. 1H NMR(300 MHz, CDCl$_3$) δ 1.67–1.74 (m, 4H, CH$_2$CH$_2$CH$_2$CH$_2$N), 2.62(t, J = 6.8, 2H, CH$_2$CH$_2$CH$_2$CH$_2$N), 4.16(t, J = 6.6, 2H, CH$_2$CH$_2$CH$_2$CH$_2$N), 7.06–7.16(m, 5H, ArH), 7.69(t, J = 7.1, 2H, ArH), 8.16(d, J = 7.4, 2H, ArH), 8.53(dd, J = 7.2, 2H, ArH). HRMS: Obs. M + H, 329.1413. Calc. M + H, 329.1416.

2-(4-Hydroxyphenethyl)-1H-benzo[de]isoquinoline-1,3(2H)-dione(7) mp:216–217°C; 1H NMR(300 MHz, CDCl$_3$) δ 2.96 (m, 2H, CH$_2$CH$_2$N), 4.36(m, 2H, CH$_2$CH$_2$N), 4.62(s, 1H, OH), 6.80(d, J = 7.5, 2H, ArH), 7.21(d, J = 7.5, 2H, ArH), 7.77(t, J = 7.2, 2H, ArH), 8.23(d, J = 7.2, 2H, ArH), 8.61(d, J = 7.2, 2H, ArH). HRMS: Obs. M + H, 318.1135. Calc. M + H, 318.1130.

2-(3,4-Dihydroxyphenethyl)-1H-benzo[de]isoquinoline-1,3(2H)-dione(8) mp:239–240°C; 1H NMR(300 MHz, CDCl$_3$) δ 2.92(m, 2H, CH$_2$CH$_2$N), 4.36(m, 2H, CH$_2$CH$_2$N), 6.81(s, 2H, ArH), 6.88(shoulder peak, 2H, OH), 6.91(s, 1H, ArH), 7.77(t, J = 7.2, 2H, ArH), 8.23(d, J = 8.1, 2H, ArH), 8.61(d, J = 7.2, 2H, ArH). HRMS: Obs. M + H, 334.1080. Calc. M + H, 334.1079.

4.3 | Preparation of Aβ monomer

Lyophilized Aβ peptide (Anaspec, Fremont, CA) was stored desiccated at −20°C until reconstitution in 50 mM NaOH at a concentration of 2 mg/mL to minimize the formation of small aggregates. Remaining aggregates were excluded via size-exclusion chromatography (SEC) on a Superdex 75 HR 10/300 column (GE Healthcare, Piscataway, NJ). Bovine serum albumin of 2 mg/mL (EMD Biosciences, San Diego, CA) was employed as a pretreatment to reduce nonspecific Aβ interaction with the dextran matrix of the column. Using a running buffer of 40 mM Tris–HCl (pH 8.0), the elution profile showed a characteristic peak corresponding to monomeric Aβ. Aβ monomer concentrations were determined with a calculated extinction coefficient of 1,450 M^{-1} cm^{-1} at 276 nm. Purified Aβ monomer samples were used fresh or stored at 4°C for up to 4 days.

4.4 | Preparation of soluble Aβ aggregate

To produce Aβ soluble aggregates, purified monomeric Aβ (up to 100 μM) was incubated with 40 mM Tris–HCl (pH 8.0) containing 3 mM NaCl at room temperature. Solutions were agitated vigorously by continuous vortexing (800 rpm) to promote assembly, and aggregation was monitored by ThT fluorescence. Soluble aggregates were separated from fibrils via centrifugation (10 min, 18,000 g) and from unreacted monomers via SEC on a Superdex 75 column, where soluble aggregates eluted in the void volume (8–10 mL). Concentrations of Aβ soluble aggregates, expressed in monomer units, were determined from UV absorbance at 276 nm corrected for light scattering, and equivalent ThT fluorescence measurements were assessed. Measurement of soluble aggregate size via dynamic light scattering (DLS) using a DynaPro-MSX instrument (Wyatt Technology Corporation, Santa Barbara, CA) revealed that this procedure consistently yielded soluble Aβ soluble aggregates displaying an average hydrodynamic radius (R_H) of ∼80 nm. Aβ soluble aggregates were stored at 4°C for up to 3 days. Following storage, ThT fluorescence measurements were used to correct for any change in soluble Aβ aggregate concentration, and DLS measurements were used to ensure that soluble aggregates maintained their initial size.

4.5 | Aβ monomer aggregation assay

Reaction mixtures of 400 μL containing 20 μM SEC-isolated Aβ monomer, 150 mM NaCl, 40 mM Tris–HCl (pH 8.0), 5% (v/v) DMSO, and selected concentrations of naphthalimide analogs were prepared in 1500 μL nonstick microtubes at room temperature (25°C). Reactions containing 0 μM naphthalimide analogs served as the positive control. Reactions were incubated under continuous agitation to enhance Aβ aggregation. During the time course of aggregation, 20 μL aliquots were periodically taken from the reaction solution and combined with 140 μL of 10 μM ThT for ThT fluorescence measurement. When associated with β-sheet structures of Aβ, ThT will give rise to a new excitation maximum at 450 nm and enhanced emission at 482 nm, in comparison with the excitation at 385 nm and emission at 445 nm of unbound ThT. Measurements were monitored using an LS-45 luminescence spectrometer (PerkinElmer Inc., Waltham, MA) with excitation at 450 nm and emission from 470 to 500 nm. Results were reported by calculating the area under the fluorescence emission spectrum curve (F) and were corrected by subtracting the ThT background. Data are reported as the change in normalized F (NF) with time, where NF is the ratio of the experimental value of fluorescence to the value of plateau fluorescence in the absence of inhibitor.

4.6 | Molecular modeling

All the ligands were generated using the sketcher in the Accelrys Discovery Studio Client 2.5 molecular modeling package. All the hydrogen atoms were added to define the correct ionization and tautomeric states. The CHARMm force field was then applied to the each molecule to assign atom types and partial charges prior to saving in .dsv format. The "Smart Minimizer" energy minimization algorithm was used for the minimization procedure with a 0.1 kcal/(mol × Å) energy gradient during a maximum 2000-step cycle of minimization. The

"AlignToSelectedSubstructure" protocol was utilized to align the compounds based the common substructure.

4.7 | Soluble Aβ aggregate elongation assay

SEC-isolated Aβ soluble aggregates of 2 μM in 40 mM Tris–HCl (pH 8.0) were combined with 80 μM of compound 8 and incubated at room temperature without agitation for 15 min to allow binding of compound 8 and soluble aggregates. Soluble aggregate elongation was initiated by the addition of 30 μM SEC-isolated monomer and periodically monitored using DLS. Reactions conducted in the absence of compound 8 served as the positive control. Experiments in which R_H of soluble aggregates was monitored in the absence of added monomers or in which R_H of monomers was monitored in the absence of added soluble aggregates served as negative controls and reflected the stability of Aβ soluble aggregate and monomer, respectively. Soluble aggregate growth was monitored as an increase in R_H using DLS. Results are reported as the change in R_H with time. Elongation rates were determined by regression of the linear portion of this data. The percentage inhibition was calculated from the ratio of the experimental elongation rate to the elongation rate observed in the absence of compound 8.

4.8 | Soluble Aβ aggregate association assay

2 μM SEC-isolated $Aβ_{1-40}$ soluble aggregates in 40 mM Tris–HCl (pH 8.0) were combined with 10 μM filtered compound 8 and incubated without agitation at 25°C for 15 min to allow binding. Soluble aggregate growth via association was initiated by addition of concentrated NaCl for a final concentration of 150 mM NaCl and periodically monitored by measurement of the increase in soluble aggregates R_H using DLS. Reactions containing 0 μM compound 8 served as the positive control. Experiments in which R_H of $Aβ_{1-40}$ soluble aggregates was monitored in the absence of added NaCl served as a negative control and reflected the stability of the $Aβ_{1-40}$ soluble aggregates. Results are reported as the increase in R_H with time. Association rates were determined by regression of the linear portion of this data. The percentage inhibition was calculated from the ratio of the experimental association rate to the association rate observed in the absence of inhibitory.

4.9 | Transmission electron microscopy

Aβ monomers of 20 μM were incubated with 150 mM NaCl in the presence of 100 μM compound 8 under agitation. After aggregation reached a plateau, which was recognized by ThT fluorescence of the control reaction, gridded samples were prepared and imaged. A 20 μL sample containing aggregated Aβ was placed upon a formvar-supported nickel grid (Electron Microscope Sciences, Hatfield, PA) and allowed to adsorb for 2 min. Sample application was repeated in this manner until the control grid contained a sufficient quantity of sample for visualization. The gridded sample was then stained with 2% filtered uranyl acetate (Electron Microscope Sciences, Hatfield, PA) for 8 min. The staining solution was wicked away from the grid edge, and the grid as allowed to air dry overnight. The dried grid was visualized using a JEOL 200CX transmission electron microscope (JEOL, Peabody, MA) at 120 kV.

4.10 | Oxygen radical absorbance capability (ORAC) assay

The OxiSelect™ Oxygen Radical Antioxidant Capacity (ORAC) Activity Assay was used to determine the antioxidant capacity of naphthalimide analogs. Briefly, 25 μL of the sample or standard and 150 μL of the ×1 fluorescein probe, prepared in assay diluent, were added to each well and incubated at 37°C for 30 min. After incubation, 25 μL of free radical initiator solution was added. A Synergy 2 plate reader measured the fluorescence of the samples at an excitation wavelength of 480 nm and an emission wavelength of 520 nm every minute for 90 min at a constant temperature of 37°C. The area under the curve (AUC) of the blank was subtracted from all other AUC values to get the net AUC. Using the equation from the trend line the net AUC value of each sample could be used to obtain the equivalent Trolox concentration of the sample. This value was then divided by the concentration of the sample and reported as the ORAC value where the standard, Trolox, has an ORAC value of 1.

4.11 | The expression of iNOS assay

The murine macrophage cell line (ANA-1 cells) was incubated for 12 hr vehicle (1% DMSO), or compound 7 (100 μM), or compound 8 (100 μM), washed, then exposed to IFN-γ (100 U/mL) for 0, 2, 4 and 8 hr. Cell lysates were analyzed by western blot analysis as described previously (Ying et al., 2005).

4.12 | MTT assay for neuroprotective activities

Cortical neuronal cultures were derived from the cerebral cortex of Sprague–Dawley rat embryos (E17-18). Briefly, cells dissociated from the cerebral cortex of embryos were seeded at a density of 5×10^5 cells/mL onto poly-D-lysine pre-coated 96-well plates for neuronal MTT assay. In the experiments, neurons were pre-treated with compound 8 alone (10 nM, 100 nM, 1 μM, 10 μM, and 100 μM) for 24 hr. The cells were washed and then challenged with 200 nM Aβ for another 24 hr. For each condition described above, a total of 2–4 independent experiments were performed with seven replicates per drug concentration evaluated. Cell viability was determined using a commercially available MTT (3-[4,5-dimethylthiazol-2-yl]-2,5 diphenyl tetrazolium bromide) assay (Invitrogen Vybrant® MTT Cell Proliferation Assay Kit). Differences were analyzed for statistical significance

using one-way ANOVA, followed by Holm-Sidak post hoc comparisons. Significance was set at $p < .05$.

ORCID

Jie Gao https://orcid.org/0000-0001-5951-1399

REFERENCES

Byun, J. H., Kim, H., Kim, Y., Mook-Jung, I., Kim, D. J., Lee, W. K., & Yoo, K. H. (2008). Aminostyrylbenzofuran derivatives as potent inhibitors for Abeta fibril formation. *Bioorganic & Medicinal Chemistry Letters*, *18*(20), 5591–5593.

Carreiras, M. C., Mendes, E., Perry, M. J., Francisco, A. P., & Marco-Contelles, J. (2013). The multifactorial nature of Alzheimer's disease for developing potential therapeutics. *Current Topics in Medicinal Chemistry*, *13*(15), 1745–1770. Retrieved from. http://www.ncbi.nlm.nih.gov/pubmed/23931435

Cavalli, A., Bolognesi, M. L., Minarini, A., Rosini, M., Tumiatti, V., Recanatini, M., & Melchiorre, C. (2008). Multi-target-directed ligands to combat neurodegenerative diseases. *Journal of Medicinal Chemistry*, *51*(3), 347–372. https://doi.org/10.1021/jm7009364

Feng, Y., & Wang, X. (2012). Antioxidant therapies for Alzheimer's disease. *Oxidative Medicine and Cellular Longevity*, *2012*, 472932–472917. https://doi.org/10.1155/2012/472932

Ghose, A. K., Herbertz, T., Hudkins, R. L., Dorsey, B. D., & Mallamo, J. P. (2012). Knowledge-based, central nervous system (CNS) lead selection and lead optimization for CNS drug discovery. *ACS Chemical Neuroscience*, *3*(1), 50–68. https://doi.org/10.1021/cn200100h

Goedert, M., & Spillantini, M. (2006). A century of Alzheimer's disease. *Science*, *314*(5800), 777–781. https://doi.org/10.1126/science.1132814

Goyal, D., Kaur, A., & Goyal, B. (2018). Benzofuran and indole: Promising scaffolds for drug development in Alzheimer's disease. *ChemMedChem*, *13*(13), 1275–1299. https://doi.org/10.1002/cmdc.201800156

Guntert, A., Dobeli, H., & Bohrmann, B. (2006). High sensitivity analysis of amyloid-beta peptide composition in amyloid deposits from human and PS2APP mouse brain. *Neuroscience*, *143*(2), 461–475.

Hardy, J., & Allsop, D. (1991). Amyloid deposition as the central event in the aetiology of Alzheimer's disease. *Trends in Pharmacological Sciences*, *12*(10), 383–388.

Kamal, A., Bolla, N. R., Srikanth, P. S., & Srivastava, A. K. (2013). Naphthalimide derivatives with therapeutic characteristics: A patent review. *Expert Opinion on Therapeutic Patents*, *23*(3), 299–317. https://doi.org/10.1517/13543776.2013.746313

Kaur, A., Mann, S., Kaur, A., Priyadarshi, N., Goyal, B., Singhal, N. K., & Goyal, D. (2019). Multi-target-directed triazole derivatives as promising agents for the treatment of Alzheimer's disease. *Bioorganic Chemistry*, *87*, 572–584. https://doi.org/10.1016/j.bioorg.2019.03.058

Kaur, A., Shuaib, S., Goyal, D., & Goyal, B. (2020). Interactions of a multifunctional di-triazole derivative with Alzheimer's Abeta42 monomer and Abeta42 protofibril: A systematic molecular dynamics study. *Physical Chemistry Chemical Physics*, *22*(3), 1543–1556. https://doi.org/10.1039/c9cp04775a

Kovacsova, M., Barta, A., Parohova, J., Vrankova, S., & Pechanova, O. (2010). Neuroprotective mechanisms of natural polyphenolic compounds. *Activitas Nervosa Superior Rediviva*, *52*(3).181–186.

Kroth, H., Ansaloni, A., Varisco, Y., Jan, A., Sreenivasachary, N., Rezaei-Ghaleh, N., … Muhs, A. (2012). Discovery and structure activity relationship of small molecule inhibitors of toxic beta-amyloid-42 fibril formation. *The Journal of Biological Chemistry*, *287*(41), 34786–34800. https://doi.org/10.1074/jbc.M112.357665

Lee, J. H., Byeon, S. R., Lim, S. J., Oh, S. J., Moon, D. H., Yoo, K. H., … Kim, D. J. (2008). Synthesis and evaluation of stilbenylbenzoxazole and stilbenylbenzothiazole derivatives for detecting beta-amyloid fibrils. *Bioorganic & Medicinal Chemistry Letters*, *18*(4), 1534–1537.

Mattson, M. P. (2004). Pathways towards and away from Alzheimer's disease. *Nature*, *430*(7000), 631–639.

McKoy, A. F., Chen, J., Schupbach, T., & Hecht, M. H. (2012). A novel inhibitor of amyloid beta (Abeta) peptide aggregation: From high throughput screening to efficacy in an animal model of Alzheimer disease. *The Journal of Biological Chemistry*, *287*(46), 38992–39000. https://doi.org/10.1074/jbc.M112.348037

Narlawar, R., Baumann, K., Schubenel, R., & Schmidt, B. (2007). Curcumin derivatives inhibit or modulate beta-amyloid precursor protein metabolism. *Neurodegenerative Diseases*, *4*(2–3), 88–93.

Nichols, M. R., Moss, M. A., Reed, D. K., Lin, W. L., Mukhopadhyay, R., Hoh, J. H., & Rosenberry, T. L. (2002). Growth of beta-amyloid (1-40) protofibrils by monomer elongation and lateral association. Characterization of distinct products by light scattering and atomic force microscopy. *Biochemistry*, *41*(19), 6115–6127.

Nie, Q., Du, X. G., & Geng, M. Y. (2011). Small molecule inhibitors of amyloid beta peptide aggregation as a potential therapeutic strategy for Alzheimer's disease. *Acta Pharmacologica Sinica*, *32*(5), 545–551. https://doi.org/10.1038/aps.2011.14

Ono, K., Hasegawa, K., Naiki, H., & Yamada, M. (2004). Curcumin has potent anti-amyloidogenic effects for Alzheimer's beta-amyloid fibrils in vitro. *Journal of Neuroscience Research*, *75*(6), 742–750.

Padurariu, M., Ciobica, A., Hritcu, L., Stoica, B., Bild, W., & Stefanescu, C. (2010). Changes of some oxidative stress markers in the serum of patients with mild cognitive impairment and Alzheimer's disease. *Neuroscience Letters*, *469*(1), 6–10. https://doi.org/10.1016/j.neulet.2009.11.033

Patil, P., Thakur, A., Sharma, A., & Flora, S. J. S. (2019). Natural products and their derivatives as multifunctional ligands against Alzheimer's disease. *Drug Development Research*, *81*, 165–183. https://doi.org/10.1002/ddr.21587

Placzek, A. T., Ferrara, S. J., Hartley, M. D., Sanford-Crane, H. S., Meinig, J. M., & Scanlan, T. S. (2016). Sobetirome prodrug esters with enhanced blood-brain barrier permeability. *Bioorganic & Medicinal Chemistry*, *24*(22), 5842–5854. https://doi.org/10.1016/j.bmc.2016.09.038

Reinke, A. A., & Gestwicki, J. E. (2007). Structure-activity relationships of amyloid beta-aggregation inhibitors based on curcumin: Influence of linker length and flexibility. *Chemical Biology & Drug Design*, *70*(3), 206–215.

Su, B., Wang, X., Nunomura, A., Moreira, P. I., Lee, H. G., Perry, G., … Zhu, X. (2008). Oxidative stress signaling in Alzheimer's disease. *Current Alzheimer Research*, *5*(6), 525-532. Retrieved from http://www.ncbi.nlm.nih.gov/pubmed/19075578

Thomas, J. D., Majumdar, S., & Sloan, K. B. (2009). Soft alkyl ether prodrugs of a model phenolic drug: The effect of incorporation of ethyleneoxy groups on transdermal delivery. *Molecules*, *14*(10), 4231–4245. https://doi.org/10.3390/molecules14104231

Tjernberg, L. O., Naslund, J., Lindqvist, F., Johansson, J., Karlstrom, A. R., Thyberg, J., … Nordstedt, C. (1996). Arrest of beta-amyloid fibril formation by a pentapeptide ligand. *The Journal of Biological Chemistry*, *271*(15), 8545–8548.

Valiveti, S., Paudel, K. S., Hammell, D. C., Hamad, M. O., Chen, J., Crooks, P. A., & Stinchcomb, A. L. (2005). In vitro/in vivo correlation of transdermal naltrexone prodrugs in hairless Guinea pigs. *Pharmaceutical Research*, *22*(6), 981–989. https://doi.org/10.1007/s11095-005-4593-0

Walsh, D. M., & Selkoe, D. J. (2007). A beta oligomers - a decade of discovery. *Journal of Neurochemistry*, *101*(5), 1172–1184. https://doi.org/10.1111/j.1471-4159.2006.04426.x

Xie, S. Q., Li, Q., Zhang, Y. H., Li, Z., Zhao, J., & Wang, C. J. (2012). BND-12, a novel nonhaematotoxic naphthalimide derivative, inhibits tumour growth and metastasis of hepatocellular carcinoma. *The Journal of Pharmacy and Pharmacology*, *64*(10), 1483–1490. https://doi.org/10.1111/j.2042-7158.2012.01519.x

Yang, Z., Song, Q., Cao, Z., Yu, G., Liu, Z., Tan, Z., & Deng, Y. (2020). Design, synthesis and evaluation of flurbiprofen-clioquinol hybrids as multitarget-directed ligands against Alzheimer's disease. *Bioorganic & Medicinal Chemistry*, *28*(7), 115374. https://doi.org/10.1016/j.bmc.2020.115374

Yiannopoulou, K. G., & Papageorgiou, S. G. (2013). Current and future treatments for Alzheimer's disease. *Therapeutic Advances in Neurological Disorders*, *6*(1), 19–33. https://doi.org/10.1177/1756285612461679

Ying, L., Marino, J., Hussain, S. P., Khan, M. A., You, S., Hofseth, A. B., ... Hofseth, L. J. (2005). Chronic inflammation promotes retinoblastoma protein hyperphosphorylation and E2F1 activation. *Cancer Research*, *65*(20), 9132–9136. https://doi.org/10.1158/0008-5472.CAN-05-1358